Wireless Sensor Networks for Pharmaceutical Lyophilization: Quantification of Local Gas Pressure and Temperature in Primary Drying

Andrew Strongrich[1] and Alina Alexeenko[1,2]

[1]*School of Aeronautical and Astronautical Engineering, Purdue University, West Lafayette, IN 47906*
[2]*Davidson School of Chemical Engineering, Purdue University, West Lafayette, IN 47906*

Keywords: Lyophilization, Freeze-drying, Wireless Sensors, Process Analytical Technologies, Computational Modeling, Fluid Dynamics

Abstract

Wireless sensor networks have become prolific in a wide range of industrial processes and offer several key advantages over their wired counterparts in terms of positioning flexibility, modularity, interconnectivity, and data routing. We demonstrate their utility in pharmaceutical lyophilization by developing a series of wireless devices to measure spatial variations in gas pressure and temperature during primary drying. The influence of shelf temperature, chamber pressure, excipient concentration, and dryer configuration are explored for various representative cycles using a laboratory-scale pharmaceutical lyophilizer. Pressure and temperature variations across the shelf for these cases are shown to vary up to 1.2 Pa and 10°C, respectively. Experimental measurements are supported by computational fluid dynamics simulations to reveal the mechanisms driving the vapor flow. The measurements and simulation data are then combined to estimate the shelf-wise sublimation rate in the inverse sense to within a deviation of 3% based on comparison with gravimetric data. We then apply the sublimation rate profile to obtain the vial heat transfer coefficient and product mass transfer resistance for a 5% w/v mannitol formulation. Finally, these parameters are applied to a 1-dimensional quasi-steady heat transfer model to predict the evolution of the product temperature over the course of primary drying. Thermocouple measurements of product temperature are compared directly to the simulated data and demonstrate accuracy comparable to existing published one-dimensional models.

Introduction

Lyophilization is a desiccation technique used to stabilize sensitive drug or food products in preparation for long-term storage. First applied on a production scale to meet the frontline demands for blood plasma, supplements, and therapeutic agents during World War II, the process has remained fundamentally unchanged to this day [1]. Traditional pharmaceutical lyophilization is a batch-mode process that takes place on temperature-controlled shelves inside of a vacuum chamber. In most cases, the drying operation proceeds in an open-loop manner. That is, pre-programmed pressure and temperature setpoints are executed sequentially at specific times during the cycle until the expected product moisture content is achieved. This “recipe” is often developed on small-scale laboratory lyophilizers which have substantially different heat and mass transfer characteristics relative to production equipment [2, 3]. Uncertainties arising from scale-up are typically accounted for by using unnecessarily conservative cycles to ensure both the product and equipment capability limits are not exceeded. The application of mathematical

modeling has helped bridge this gap and accelerate cycle development. However, theoretical treatments alone are insufficient and must be supplemented by physical measurements to improve the robustness of current Process Analytical Technologies (PAT).

Numerous technologies have been proposed to measure or estimate drying performance throughout the lyophilization process. The reader is referred to a survey by Fissore et al. for an exhaustive summary [4]. Of the documented PAT methods, few are simultaneously practical in production environments, non-invasive, and able to provide spatially resolved measurements of the variable of interest. Wireless Sensor Networks (WSNs) are ideal candidates to overcome these limitations and are well-established in a variety of industrial applications [5]. The key advantage to WSNs is their high degree of positioning flexibility and modularity, allowing the operator to monitor specific process variables of interest in real time at nearly any location within the lyophilizer. This capability is highly advantageous, especially in production settings where accessibility is limited due to tightly regulated cGMP aseptic manufacturing protocols [6]. Two of the most critical variables in any lyophilization process include the gas pressure and temperature, both of which can vary significantly throughout the process chamber.

Pressure and temperature variations within the shelf networks of lyophilizers have been well-documented using a variety of analytical and numerical approaches. In 1971, Massey developed a 2-dimensional model of a semiporous channel to describe the distributions of gas pressure and product temperature along the length of the shelf in an industrial-scale freeze-dryer assuming the product exhibits a uniform sublimation rate. The model was compared to experimental measurements collected from haddock drying with a high degree of accuracy [7, 8]. Variations of Massey's model have been developed (which are also applicable outside of freeze-drying) and generalize the injection boundary assumptions to include non-uniform profiles or 3-dimensional channels [9, 10]. A simplified analytical approach to the semiporous injection system was developed by Zhang who created a model to estimate the variation of water vapor pressure throughout the lyophilizer process chamber [11]. The solution is based on Poiseuille (pressure-driven) flow and includes an additional profile stretching term to account for the boundary mass injection. Although these analytical approximations are useful for developing an understanding of the relationship between local gas pressure or temperature and product state, they are unable to account for the complex 3-dimensional geometries (e.g. vials and stoppers) found in real lyophilization systems.

Computational Fluid Dynamics (CFD) allows many of the limitations associated with analytical methods to be overcome by simultaneously offering a high degree of flexibility, versatility, and accuracy. Numerous studies have applied CFD to the lyophilization process to describe the flow behavior at various locations throughout the system including the condenser chamber [12, 13], duct [14, 15], and process chamber [6, 16, 17, 18, 19, 20, 21]. Rasetto developed a dual-scale model using a combination of CFD and an analytical description of the vial sublimation and heat transfer characteristics to model heterogeneity in production-scale lyophilizers [20, 21]. Barresi later adapted the model to include gas mixtures and examined the effects of low-pressure boundary slip in both production and laboratory environment. The pressure drop across the shelf was shown to vary linearly with sublimation rate for a fixed base pressure [17]. Similar results were obtained by Ganguly who investigated flow behavior in a laboratory-scale lyophilizer using a multi-species model to determine the parameters that contribute to pressure variation along the shelf [18]. The sublimation surface was assumed to be an ice slab having uniform temperature and sublimation rate. The results were compared to experimental measurements of the pressure

difference between the center of a laboratory-scale lyophilizer and the edge. These tests employed an ice slab and false shelf inserted above the slab containing two pressure taps. The differential pressure measurement was shown to exhibit dependence on chamber pressure, shelf temperature, and the distance between the sublimation surface and shelf above [22]. In particular, the pressure difference was shown to be highly sensitive to the shelf spacing and varied in inverse proportion with this parameter.

The impact on spatial variations of gas pressure on drying performance at both the laboratory and production scales was briefly addressed by Sane [22]. In the laboratory, the pressure variations are small relative to the base pressure and can generally be neglected. This behavior has been confirmed experimentally using different shelf gap heights [23]. At the large length scales encountered in manufacturing, the pressure variations increase significantly which can lead to nonuniformities in heat transfer characteristics. In some cases, these variations can be large enough to produce a higher drying rate in center vials due to the modulation of the vial heat transfer coefficient. In this way, the pressure variations can be desirable and even utilized to offset the edge vial effect.

This work aims to provide spatially resolved experimental measurements of gas pressure and temperature in real time within the vial pack during primary drying. The study supplements existing numerical models and experimental data by performing quantitative measurements of pharmaceutical formulations under various process conditions over the entire shelf surface. The measurements are collected using a series of custom fabricated wireless gas vacuum and temperature sensors located within the vial network. The measurements are compared to CFD models to develop a deeper understanding of flow behavior. The shelf-averaged sublimation rate over the course of primary drying is estimated by applying the CFD solution to the experimental pressure and temperature data, ultimately setting the stage to empirically evaluate heat and mass transfer characteristics in a non-invasive way.

Materials and Methods

Lyophilization Cycle Parameters

All tests were conducted in a REVO® (Millrock, Kingston, NY) laboratory-scale lyophilizer. A summary of the formulations and process parameters used in the experiments is shown in Table 1. UPW indicates ultra-pure water (purified and verified in-house) having resistivity of > 18.2 MΩ-cm and was used as the solvent in all tests. The excipient was either sucrose (Sigma-Aldrich, St. Louis, MO) or D-mannitol (Phansteil, Waukegan, IL), both having concentrations of 5% w/v. Experiments were performed using 201 20cc type 1 glass tubing vials (Schott, Lebanon, PA) with a 5 mL fill volume. This vial quantity corresponds to one fully-loaded shelf with sensors included. Product temperature measurements were performed using two 40 gauge T-type thermocouples (Omega Engineering, Norwalk, CT). Both thermocouples were placed in center vials and one was located adjacent to one of the wireless sensors to evaluate the influence of parasitic heating from the device housing.

Wireless Pirani Sensor Design

The pressure and temperature within the lyophilizer were measured using an array of six custom-fabricated Wireless MicroPirani (WMP) sensors. The sensing element for each device consisted of a silicon die with two metal filaments, one deposited on a suspended diaphragm acting as the Pirani filament and the other on the substrate as a Resistance Temperature Detector (RTD). The

Pirani filament reacted to changes in ambient gas pressure, composition, and temperature and the RTD was used to both measure ambient gas temperature and compensate for its variation over the course of drying. It is assumed that the Pirani and RTD elements are in thermal equilibrium with the gas temperature over the course of the drying cycle.

The Pirani and RTD sensors were biased using a self-balancing bridge architecture, ensuring the Pirani filament temperature always maintained a constant offset of around 10°C relative to the ambient. The power needed to maintain the filament at the target temperature and pressure was used to resolve gas pressure. The devices were battery powered and had a nominal lifetime of around 70 hours. The sensors were encapsulated in a package having the same footprint as a 20cc glass tubing vial. The height was selected such that the system is undamaged during stoppering operations. An image of the devices and their placements within the vial pack is provided in Figure 1. The locations of the sensors were preserved between all tests unless otherwise noted. Location independence has been verified by performing duplicate experiments with the sensors in different locations. All devices read within the calibration uncertainty of +/- 0.03 Pa relative to their counterpart when changing positions. During the tests, pressure and temperature measurements were broadcast from each device in real time and logged on a host PC located near the lyophilizer. Measurements were sampled with 24-bit precision and broadcast to the host at a sampling interval of 5 seconds (0.2 Hz). Supplementary temperature measurements were carried out using two 30 gauge T-type thermocouples (Omega Engineering, Norwalk, CT). These probes measured the outside wall temperatures of WMP4's housing and an isolated center vial 2 cm from their bases, respectively.

Calibration

The WMP sensors correlate power dissipation of the heated filament to ambient pressure and are therefore highly sensitive to the thermal conductivity of the gas. Typically, Pirani gauges used in lyophilization are calibrated in pure nitrogen and are used to provide a rough indication of composition during primary and secondary drying when compared to an absolute measurement from a capacitance manometer [24]. It has been shown both computationally and experimentally that the composition of the gas in the chamber during primary drying is nearly completely water vapor. [25, 26, 27] Therefore, to measure pressure in the absolute sense, the WMP devices were calibrated in a similar environment.

The WMP calibration was performed by mounting the devices to an aluminum fixture and placing it in contact with the lyophilizer shelf. The temperature of the fixture was monitored throughout the entire process using two 30 gauge T-type thermocouples to ensure equilibrium at the shelf temperature setpoint before pressure stepping was initiated. Water vapor pressure was regulated by feeding sublimed vapor in from an external chamber via a custom motorized proportional valve. The lyophilizer's capacitance manometer (MKS Baratron® 626C, Andover, MA) had a full-scale range of 2 Torr and provided the necessary feedback to the vapor controller in terms of absolute pressure. Vapor flow through the lyophilizer's duct was restricted using a custom machined plug, reducing the diameter from 125mm to 8 mm. Under these low flow rate conditions, it is reasonable to assume that pressure variations throughout the process chamber are negligible and the calibration is insensitive to the placement of the capacitance manometer. Gas composition was monitored via a Transpector® CPM3 residual gas analyzer (Inficon, Syracuse, NY) mounted on the top of the process chamber, demonstrating an average water vapor concentration of approximately >99% throughout the entire process. Temperature setpoints of -33 to 33°C in increments of 11°C were applied to be representative of typical lyophilization cycles while also

preventing water vapor from frosting on the devices at the higher pressure setpoints. At each temperature, the pressure was varied from 6.7 Pa to 20 Pa in increments of 0.7 Pa and averaged at each point for 5 minutes. The data collected during the calibration procedure forms a 3-dimensional surface of points that was fit with a third-order bivariate spline. A unique spline surface was generated for each device and applied to the measurements conducted during the lyophilization cycles to evaluate local pressure. In this way, the devices are independent of the lyophilizer and only depend on the accuracy of the reference pressure gauge. Nevertheless, the sensors were only used in the lyophilizer in which they were calibrated, making small long-term drift errors in the capacitance manometer irrelevant.

Theoretical Development

Flow within the shelf network was modeled using the commercial software package Fluent (ANSYS, Canonsburg, PA). The incompressible 3-dimensional Navier-Stokes equations were solved using a pressure-based steady-state solver with full pressure-velocity coupling and second-order upwind differencing. Buoyancy effects were neglected, and the gas was assumed to be pure water vapor. The flow was also assumed to be laminar and a low-pressure velocity and temperature slip correction with unity accommodation (thermal and momentum) was applied to all solid boundaries. Justification for these models can be made through consideration of the relevant non-dimensional flow variables, namely the Reynolds (O(1)) and Knudsen (O(0.01)) numbers [6].

A schematic of the computational domain is presented in Figure 2. The fluid viscosity, heat capacity, and thermal conductivity were determined from the literature and computed using thermocouple data [28]. A total of 201 vials were modeled and a uniform mass flux was applied at the ice/vapor interface. The outlets were assigned a constant pressure equal to that of the measured chamber pressure. The product, vial wall, shelf, and side wall temperatures were assigned based on thermocouple measurements. A mesh sensitivity study was performed prior to simulation across four meshes of increasing cell density and the criterion was based on the relative change in pressure magnitude at the center of the shelf. The mesh selected for the simulations contained 15.7 million elements and a scaled residual convergence for continuity, momentum, and energy of at least 1e-5 was achieved in all cases.

The sublimation rate represents the unknown variable during modeling and was determined using an iterative minimization process. First, the boundary temperatures were applied using thermocouple data at a given time instant during the cycle. From here, a series of simulations were performed at different mass flow rates ranging from 0.018 g/hr/vial to 0.627 g/hr/vial and the pressure at each of the sensor locations, $p_{i,CFD}$, was evaluated and compared to the experimentally measured values from the WMP devices, $p_{i,meas}$, in the form of the root-mean-square deviation, σ.

$$\sigma = \sqrt{\frac{1}{N}\sum_{i=1}^{N}\left(p_{i,CFD} - p_{i,meas}\right)^2} \tag{1}$$

where N is the number of sensors and p is the pressure, either modeled or measured, at each of the sensor locations. The discrete mass flow rates and errors were then fit with a third-order interpolating spline and the location of the minimum was assumed to be the best estimate for the sublimation rate at the considered instant of time. This process was repeated at several discrete

times throughout primary drying, allowing the temporal evolution of the mass flux to be determined. Using this information, the product heat and mass transfer characteristics were then evaluated.

Several mathematical models have been developed to describe the evolution of the product temperature during primary drying [29, 30, 31, 32]. One common technique is to apply the assumption of a quasi-steady zero-dimensional system. In this case, the rate of energy change in the frozen volume, e, in the product is simply given by

$$\frac{de}{dt} = 0 = K_v A_v (T_s - T_b) - \dot{m}_{sub} H_{sub} \tag{2}$$

where K_v is the vial heat transfer coefficient, A_v is the vial cross sectional area, T_s is the shelf temperature, T_b is the temperature at the bottom of the frozen formulation, $\dot{m}_{sub}$ is the sublimation rate, and H_{sub} is the enthalpy of sublimation. The sublimation rate can be further described by pressure loss across the dry layer.

$$\dot{m}_{sub} = \frac{\left(P_{vap}(T_{sub}) - P_{ch}\right)}{R_p} A_p \tag{3}$$

Here, P_{vap} is the saturated vapor pressure at the interface, P_{ch} is the chamber pressure, R_p is the mass transfer resistance, and A_p is the product cross sectional area. In general, K_v and R_p are empirical in nature and determined through a series of experiments at varying chamber conditions. They frequently assume the forms [30, 33]

$$K_v = K_c + \frac{K_P P_{ch}}{1 + K_D P_{ch}} \tag{4}$$

$$R_p = R_0 + \frac{R_1 l}{1 + R_2 l} \tag{5}$$

The mass transfer resistance varies with the dry layer thickness, l, and can be computed over the course of drying through knowledge of the accumulated mass lost through sublimation. Coupling the WMP measurements with CFD simulation results provides the sublimation rate over the course of primary drying. With this information, computation of the heat and mass transfer coefficients is straightforward by applying a nonlinear least-squares fit to equations 2-5. After acquiring the empirical data, computation of the product temperature at the bottom of the frozen volume is carried out using the open-source tool, LyoPRONTO [29].

Results

The process data for a 5% w/v mannitol formulation with primary drying chamber pressure of 13.3 Pa and shelf temperature of 10°C (Cycle H in Table 1) are shown in Figure 3. At the onset of primary drying (at an elapsed time of 7.5) hours the pressure surrounding the vials begins to increase in response to the shelf temperature ramp. Initially, the indicated pressure is lower than the absolute measurement from the capacitance manometer (CM) due to the presence of nitrogen. During the ramp, water vapor gradually replaces the inert ballast in the shelf network and the pressure gradient from the center to the edge increases. All sensors reveal a gradual decrease in local pressure over the course of primary drying. This behavior indicates a decreasing sublimation rate and is expected since the product resistance grows as the drying process proceeds [18, 22]. Near the end of primary drying at around 18.5 hours the pressure measured

by the WMP devices begins to fall rapidly as the nitrogen ballast fills the chamber and ingresses towards the center of the shelf. Following primary drying the WMP sensors read erroneously low due to the lower thermal conductivity of nitrogen. It should be noted that WMP data in this region are extrapolated from the spline surface and therefore can be expected to exhibit an offset relative to one another. The secondary drying phase between 27 and 29 hours is met with an increase in measured pressure signal due to the desorption of water vapor from the dry layer. However, these measurements are not absolute and provide only an indication of when the secondary drying process is complete.

In terms of measured gas temperature, all devices, except WMP1 and WMP3, produce readings within an envelope of approximately 2°C over the course of primary drying. Devices 1 and 3 measure higher temperatures than the rest of the group due to radiative and convective heating action near the edge of the shelf [2]. WMP3 is closest to the edge and is therefore most affected. Thermocouples 1 and 2 were placed in the center of the vial pack to determine the effect of the WMP sensors on product temperature in adjacent vials. However, the two probes show no greater than a 2°C offset throughout the entire process. For clarity, only their average value, $T_{p,meas}$, is shown. Although some parasitic heating from the sensors can be expected, we speculate that the effect is relatively mild and the vials in contact with the sensors will finish primary drying sometime between the center and edge vials. This conclusion is based on published findings investigating the influence of the number of neighboring product vials and local product temperature [34]. Thermocouples 3 and 4 also exhibit nearly identical behavior to one another and are indicated by the average, $T_{v,meas}$.

All sensor positions indicated in Figures 1 and 2 are shifted two vial spaces along the negative y-direction and Cycle H is duplicated to develop a mapping of gas pressure and temperature over the shelf. This offset distance was chosen to both provide a measurable change in pressure magnitude while also minimizing the potential for erroneous measurement due to upstream mixing of nitrogen ballast near the perimeter. Measurements from both cycles are combined at a process time of 11 hours to form surface and contour data, both of which are shown in Figure 4. The chamber pressure of 13.3 Pa is imposed at the shelf boundaries to fill the map. Gas temperatures at the boundary locations are unknown and thus only a partial distribution could be obtained.

The data in Figure 4a demonstrate a smoothly varying pressure distribution over the area of the shelf with a maximum just aft of the center point and a minimum along the periphery. The mild asymmetry between the front and rear of the shelf is due to the outlets in the supporting sidewalls between 18 and 34 cm. These features are also visible in the contour data. The pressure gradients with respect to the y-coordinate near the outlets are 24% larger than those in the x-direction and tend to draw the vapor away from the centerline. The outlets reduce mass flow demands in the x-direction and ultimately reduce the gradient towards the front half of the shelf. Asymmetries can also arise due to the location of the duct that separates the process and condenser chambers [20]. However, in this case, the location of maximum pressure would tend to shift away from the duct. For given process conditions, pressure variations will grow with increasing shelf length and will potentially affect drying rate in a production setting where characteristic sizes are on the order of a few meters [22, 35].

The temperature data in Figure 4b indicate a minimum temperature near the location of maximum pressure. It is expected that the gas temperature increases towards the outlets due to the influence of the edge vial and convective heat transfer effects [2]. The temperature near the sidewall outlets is higher than the surrounding gas, suggesting the edge vial effect is enhanced

for samples in this area. One potential explanation for this observation is radiative transport from the chamber walls to the vials exposed by the cutout.

Effect of Shelf Temperature

Raising the shelf temperature increases the heat flow into the cake and provides additional energy to offset that which is lost through sublimation. The effect of shelf temperature on local gas pressure and temperature is shown in Figure 5 for center (WMP2) and edge (WMP3) vials (see Figure 1). All other sensor measurements fell within the envelope formed by these devices so, for clarity, they have been omitted. The cycles represented are B, C, and D in Table 1.

The pressure difference from center to edge at a fixed pressure of 9.3 Pa increases with increasing shelf temperature. This behavior can be explained by the increase in mass flow rate between the shelves. The velocity profile between the tops of the vials and the bottom of the shelf above can be roughly approximated as parabolic with a velocity magnitude of zero at the solid surfaces and average velocity defined by the mass flow requirement [11]. In the physical system, the gas rarefaction will produce a non-zero velocity at the boundary. However, this effect is temporarily neglected to simplify the discussion. As the vapor flows within this region the principle of mass conservation requires an increase in velocity and stretching of the profile. The shear stress (viscous dissipation) scales with the velocity gradient normal to the solid surfaces. Therefore, as velocity increases, the shear stress increases and the system must apply a larger pressure gradient along the length of the shelf to maintain the target mass flow rate.

The gas temperature in Figure 5 at the onset of primary drying experiences a rapid increase as the shelf temperature is raised to its target setpoint. During this period the sublimation rate is low and the heat transfer into the gas is dominated by conduction between the shelves. Once the setpoint is reached, the cold subliming water vapor enters the shelf network and begins to offset the heating, leading to a deceleration of the measured gas temperature. As primary drying proceeds, the sublimation rate decreases due to the increasing dry layer resistance and the gas temperature once again accelerates. The conclusion of primary drying is indicated by the second deceleration of the gas temperature as it approaches the shelf setpoint.

Effect of Chamber Pressure

The chamber pressure influences gas conduction heat transfer to the vial and therefore contributes significantly to the sublimation rate. The influence of gas pressure is usually determined empirically in the form of the vial heat transfer coefficient and has a nonlinear but monotonic form [30]. To observe the effect of the chamber base pressure a series of experiments using a 5% w/v sucrose formulation are carried out using cycles D, E, and F in Table 1. The experimental data is illustrated in Figure 6. Here, the pressure is expressed in terms of the gauge pressure relative to the process chamber setpoint to enable a direct comparison between experiments.

The data in Figure 6 demonstrate a direct relationship between chamber pressure and average sublimation rate as is evidenced by the relative convergence times (i.e. a precipitous drop in pressure or equilibration with the shelf temperature). The clearance between the bottom of the vials used in this study and the shelf is assumed to be on the order of a few hundred microns, making it comparable to the molecular mean free path at pressures commonly applied in lyophilization [30]. In this transitional rarefied regime, gas conduction heat transfer exhibits a nonlinear but proportional dependence on pressure which acts to modulate the heat transfer rate into the cake. For a fixed pressure, an increase in mass transfer rate was shown in Figure 5 to

increase the pressure gradient from center to edge. However, as chamber pressure increases at a constant shelf temperature the pressure difference from center to edge in Figure 6 decreases. This inverse variation with bulk density is in qualitative agreement with the analytical channel flow models with semi-porous membrane [7, 9, 11] as well as higher fidelity CFD simulations [35]. The physical explanation for this trend lies in the Reynolds number which is defined as the ratio of the inertial and viscous forces. The Reynolds number in the shelf network is on the order of unity which suggests that local turbulent fluctuations are heavily dampened by viscous effects. It can therefore be assumed that the flow exhibits purely laminar behavior. As Reynolds number is increased (e.g. by increasing density, mass flow rate, or channel height), the inertial forces grow relative to the viscous forces and the flow more readily overcomes the energy loss through viscous dissipation. As a result, at higher base pressures, a smaller pressure gradient is required to transport the given quantity of fluid from the center of the shelf to the edge.

Effect of Excipient

The excipient composition and concentration affect the mass transfer resistance and the pressure variation over the vial pack. To examine the influence of different excipients on pressure and temperature a series of tests are carried out using UPW, 5% sucrose, and 5% mannitol. These tests are indicated by cycles A, B, and G in Table 1, respectively. A comparison of measured gas pressure and temperature at the center and edge of the vial pack for each excipient over the course of lyophilization is shown in Figure 7.

The UPW samples dry most quickly due to the absence of a dry layer. The pressure difference is nearly constant over the first half of primary drying, suggesting the sublimation rate in this interval is also constant. As the ice front approaches the bottom of the vial in the latter half of primary drying it becomes hemispherical and recedes inwards towards the axis. The reduction in surface area lowers the sublimation rate and ultimately the pressure difference. The behaviors of sucrose and mannitol are also shown in Figure 7. The 5% sucrose formulation produces a drying time very close to that of pure water due to its relatively low mass transfer resistance. It has been shown that the low critical temperature of sucrose leads to microcollapse of the partially dried layer as the sublimation front progresses, resulting in a nearly linear increase in *effective* pore size with dry layer thickness [33]. In reality, microscopic holes form in the cake structure (matrix) as it transitions into a highly viscous fluid, ultimately reducing mass transfer resistance. Gas conductance in the rarefied flow regime (i.e. when the molecular mean free path is much larger than the pore diameter) is proportional to the pore diameter and inversely proportional to the channel length, resulting in competing mechanisms over the course of primary drying. The high critical temperature of mannitol formulations inhibits this effect, resulting in a constant conductance throughout the drying process. Therefore, for a given shelf temperature and chamber pressure, mannitol formulations will have increased drying times and lower sublimation rates than sucrose at similar concentrations.

Effect of Lyophilizer Configuration

Lyophilizers come in a variety of sizes and configurations at both the laboratory and production scales. One feature that has a pronounced effect on the gas pressure and temperature in the vicinity of the vials is the shelf support system (i.e. the structure used to support the shelves and control spacing). To examine the relative influence of the sidewall outlets a pair of polycarbonate flow barriers were installed along the sides of the shelf to constrain vapor flow to the axial direction only. A comparison of the flow data for cycle H that illustrates the pressure drop from center to edge with and without sidewall outlets is shown in Figure 8. Constraining the flow to move along

the length of the shelf has a significant influence on the pressure difference from center to edge, moving from a difference of 0.35 Pa in the standard configuration to 1.2 Pa with the flow barriers installed at the beginning of primary drying.

The influence of the pressure variations on heat transfer performance (in terms of the vial heat transfer coefficient) is likely on the order of a few percent based on empirical correlations provided in the literature [29, 30]. The drying rates between the two cycles are approximately the same which is inferred from relative WMP pressure convergence times (near 13 hours). It is therefore expected that both cycles will exhibit roughly the same product temperature throughout the process. The gas temperature over the course of primary drying demonstrates almost no dependence on the flow barriers within the region of the center vials, further supporting the observation that the sublimation rates for both cases are nearly identical.

To gain additional insight into the pressure and temperature distribution over the shelf the sensors were once again shifted in the y-direction and cycle H was duplicated. The results of the procedure are shown in Figure 9. The effect of the flow barriers is clearly visible in the pressure distribution. The flow is actuated by the pressure gradient, so the shape illustrates that the flow is in a purely axial direction (i.e. towards the fore and aft exits). Comparison of the contours between Figures 4a and 9a demonstrate that the location of maximum pressure for the cycle using flow barriers also lies closer to the center of the shelf.

According to Figure 9b, the flow barriers have an influence on the shape of the temperature distribution away from the centerline. Without the false walls, heat transfer from the chamber walls leads to an elevated temperature in the region of the sidewall outlets. Based on the shape of the surface, it is expected that the heat transfer rate into vials near the cutout lies somewhere between those along the solid sidewall and those at the fore and aft shelf exits. With the barriers installed, all edge vials are exposed to roughly the same heat transfer and the temperature distribution becomes largely uniform.

Computational Modeling

The influence of shelf temperature, chamber pressure, formulation, and lyophilizer configuration on the pressure and temperature distribution within the vial pack warrants further investigation in the form of computational modeling. Flowfield results for cycle H in terms of gas pressure and velocity magnitude 3.4 hours after the beginning of primary drying (11 hours elapsed) are shown in Figure 10. The estimated sublimation rate at this time is 0.475 g/hr/vial from the pressure matching procedure. To verify this estimate, two gravimetric tests were performed on cycle H. The first was stoppered 1.52 hours after the beginning of primary drying and the second was stoppered at 4.2 hours. The average sublimation rate between these times is determined to be 0.457 g/hr/vial, leading to an estimation error of 3.9%.

The vapor flow within the shelf network is actuated by the pressure gradients and will tend to follow the path of steepest descent perpendicular to the isobar contours. The directional gradients near the center of the shelf are strongest towards the sidewall outlets, causing the flow to accelerate towards these features and exit the domain. The sidewall outlets produce the highest fluid velocity upon exit relative to the other boundaries due to the sharp acceleration. In the fore and aft sections of the shelf the vapor preferentially exits in the x-coordinate directions since the axial gradients at these locations are larger than the transverse.

A comparison of the measured pressure and that which is estimated from the CFD solution at the sensor locations is shown in Figure 11. The total root-mean-square deviation between the data sets at the locations of the sensors is 0.06 Pa. Roughly 40% of the error contribution is from the sensor (WMP3) located closest to the edge of the shelf. The indicated reading was verified as repeatable by performing a duplicate experiment with a different sensor (WMP5) at this location. One possible cause for the discrepancy is the local mixing of nitrogen with the water vapor [6]. As the vapor passes over the final row of vials just upstream of the exit it encounters a strongly adverse pressure gradient and separates from the stoppers. This sets up a vortical region near the base of the vial that is sustained by the shearing action of the separated bulk flow. As the nitrogen ballast flows downwards past the aft exit of the shelf on its way to the duct it is reasonable to suggest that some of this gas mixes with the water vapor in the vortex region and gets transported a small distance upstream through the gaps between the vials close to the lower shelf. This slow moving flow would likely be drawn upwards by the static pressure difference. Due to this mixing action, the assumption of pure water vapor near the edge vial region would be expected to break down and produce an erroneously low indicated pressure. If the measurement from WMP3 is ignored, the deviation is reduced to 0.04 Pa. With WMP3 removed, most of the discrepancy is from WMP4 and WMP6. These devices are located away from the centerline where the transverse pressure gradients are large. The vial packing during experiments was somewhat loose, so it is possible that the devices shifted slightly from their nominal positions when loading the tray. The difference between the CFD solution and measurements at these locations corresponds to a position uncertainty of around 0.8 cm.

The CFD model was applied to cycle H using the polycarbonate sidewall flow barriers. The pressure and velocity magnitude flowfields 3.4 hours after the beginning of primary drying (11 hours elapsed) are shown in Figure 12. The pressure-matching procedure predicts a sublimation rate of 0.430 g/hr/vial, a 10% decrease from the case having sidewall outlets. The flow barriers force the vapor to exit the domain at the fore and aft exits and significantly reduce the transverse pressure gradients present in Figure 4a. This increases flow rate demand on the fore and aft exits and ultimately increases the shear stress and requires a larger pressure gradient for actuation.

The comparison between the CFD solution and experimental measurements at each sensor location when using the flow barriers is shown in Figure 13. The agreement between the simulation and measurements is improved by a factor of four relative to the case without the false walls, having a mean-square deviation of 0.01 Pa. The measurements from WMP3, WMP4, and WMP6 move closer to the centerline pressure due to the reduction in transverse pressure gradients.

Application of the flow matching procedure based on the pressure distribution allows the sublimation rate to be determined at any discrete point during primary drying. With this information, both the heat and mass transfer characteristics of the vial and product can be estimated and used to describe the evolution of the product temperature for arbitrary process conditions. In principle, the measured pressure and temperature can also be used to directly estimate product temperature, however such a capability would either require on-line solution of a flow model or an interpolation table containing various process conditions.

Heat and Mass Transfer Characterization

The sublimation rate is estimated over the course of primary drying by combining the experimental pressure and temperature measurements with CFD simulations. This information, with the addition of the measured product temperature, provides the necessary closure to

extract the heat and mass characteristics of the system at a given point in time. Using the relations in equations 2-5, K_v and R_p were evaluated for a 5% w/v mannitol formulation following cycle H.

$$K_v = 15.6 \left[\frac{W}{m^2 K}\right]$$

$$R_p = 1.01e5 + 7.92e7\ l \left[\frac{m}{s}\right]$$

The heat transfer coefficient was computed at the constant chamber base pressure of 13.3 Pa by averaging over each point in time. In general, the magnitude of K_v will exhibit nonlinear behavior with pressure and requires additional experiments or a variable chamber pressure to fully develop. However, the influence of pressure is not investigated here. The product resistance was linear as function of the dry layer length, making a fit of similar form appropriate (i.e. the coefficient, R_2, in equation 5 is set to zero). Similar variations using mannitol have been reported in the literature [30, 33]. Using the relations for K_v and R_p, the estimated sublimation rate and product temperature over the course of primary drying for cycle H (without flow barriers) are shown in Figure 14. Uncertainty bounds are indicated by the shaded regions surrounding the temperature estimate.

The estimated product temperature demonstrates good agreement with the experimental measurements over the course of primary drying, having a maximum difference of 1.1°C at an elapsed cycle time of 16 hours. The measured temperature lies within the uncertainty bounds throughout the entire cycle except for a brief period surrounding this time. We believe that the estimation error at this point is due to the development of a hemispherical sublimation surface that challenges that assumption of a constant interface area. The dry layer length reaches the fill height at a time corresponding to the onset of the Pirani gauge convergence and is indicated by the termination of the simulation data. This is also the time at which the thermocouple measurement accelerates towards the shelf temperature, suggesting nearly all of the bulk water has been removed.

Outlook and Future Improvements

The WMP sensors developed in this work successfully demonstrated the capability of measuring and broadcasting local gas pressure and temperature during primary drying in a laboratory-scale lyophilizer. Several modifications are proposed to both enable compatibility with aseptic cGMP manufacturing equipment and further enhance performance. The device enclosures were composed of acrylonitrile butadiene styrene (ABS) and would likely be incompatible with many standard sterilization techniques such as steam, dry heat, or hydrogen peroxide. Therefore, we suggest fabricating the enclosures using a more chemically and thermally resistant (but also RF-transparent) material such as Polytetrafluoroethylene (PTFE) or Polyether ether ketone (PEEK). We also recommend the enclosures be hermetically sealed prior to installation to prevent moisture ingress. If high temperature sterilization is required, it is likely that the lithium polymer batteries used in the current implementation will need to be replaced with a more temperature-tolerant energy storage system. Alternatively, the sensors may be sterilized using gamma radiation. However, the effects on the electronics module following this method are unknown. It is worth noting that the 20R enclosure footprint used in this study was chosen as a matter of fabrication convenience. The smallest feasible package based on the current iteration would have a footprint identical to a 6R vial.

In terms of performance, device efficiency can be significantly improved by incorporating duty cycling. This feature would increase battery life from the existing 70 hours to a week or more. Alternatively, if a shorter duration is acceptable, the filament may instead be run at higher power levels to increase sensitivity to changes in ambient pressure. To prove beneficial, the devices would require calibration against a higher precision reference gauge. Additionally, power dissipation should be kept at modest levels to reduce the onset of long-term drift. Pirani element drift in lyophilization can occur from a variety of sources including slow filament oxidation, mechanical strain induced by sterilization, or contamination (heat transfer modulation). In this study, no WMP sensor drift was detectable after a few dozen lyophilization cycles. Nevertheless, the low component cost allows the issue of drift to be avoided altogether by making the devices disposable. This operational model would also enable the sensors to be pre-sterilized using the most compatible method.

If the proposed modifications can be addressed, the WMP sensors have the potential to supplement and enhance existing lyophilization PAT. To the best of the authors' knowledge, there exist no experimental measurements of the water vapor pressure distribution within pilot or manufacturing scale lyophilizers. Data collected in such systems would prove highly beneficial for CFD model validation or as a PAT tool for characterizing intershelf and intrashelf drying rate variations. Eventually, gas pressure and temperature measurements could be supplemented with other wireless sensing technologies (e.g. wireless product temperature sensors) to enable closed-loop control. Several closed-loop models have already been proposed and would benefit substantially from the high spatial fidelity offered by wireless sensing technologies [16, 36, 37].

Conclusions

The ability to capture local process variables in lyophilization is critical to enhancing existing process analytical technologies. With the growing popularity of wireless sensor networks in industrial processes, this capability is now within reach. In this study, series of custom wireless microPirani sensors were designed, fabricated, calibrated, and applied to the measurement of local gas pressure and temperature within the vial pack during primary drying. The effects of shelf temperature, process pressure, formulation, and lyophilizer configuration were explored individually. Shelfwise pressure gradients demonstrated direct correlation with sublimation rate except when varying pressure. In this case, increasing pressure was met with a decrease in gradient due to the growth of the inertial forces. CFD simulations of the vial pack were performed and the results were quantitatively compared to the experimental measurements with good agreement. A pressure-matching procedure using the CFD model was then developed to estimate the sublimation rate at several discrete points over the course of primary drying. This information, in turn, was used to directly evaluate the heat and mass transfer parameters of the system and to predict the evolution of product temperature using a quasi-steady one-dimensional heat and mass transfer model. Results demonstrated a strong agreement to experimental measurements and suggests the method is a viable option for estimation of the shelf-averaged sublimation rate.

Acknowledgements

This work was funded by the National Science Foundation (NSF) Grant #1827717: Sensors, Computational Modeling, and Bioanalytical Technologies for Closed-Loop Lyophilization

References

[1] D. Varshney and M. Singh, "History of Lyophilization," in *Lyophilized Biologics and Vaccines*, New York, Springer, 2015, pp. 3-10.

[2] M. Pikal, R. Bogner, V. Mudhivarthi, P. Sharma and P. Sane, "Freeze-drying process development and scale-up: scale-up of edge vial versus center vial heat transfer coefficients, Kv," *Journal of Pharmaceutical Sciences,* vol. 105, no. 11, pp. 3333-3343, 2016.

[3] D. Fissore and A. Barresi, "Scale-up and process transfer of freeze-drying recipes," *Drying Technology,* vol. 29, no. 14, pp. 1673-1684, 2011.

[4] D. Fissore, R. Pisano and A. Barresi, "Process Analytical Technology for Monitoring Pharmaceutical Freeze-Drying-A Comprehensive Review," *Drying Technology,* vol. 36, no. 15, pp. 1839-1865, 2018.

[5] S. Ramamurthy, "Wireless Sensor Networks: Technologies and Global Markets," BCC Research, 2016.

[6] A. Barresi, V. Rasetto and D. Marchisio, "Use of Computational Fluid Dynamics for Improving Freeze-Dryers Design and Process Understanding. Part 1: Modeling of the Lyophilization Chamber," *European Journal of Pharmaceutics and Biopharmaceutics,* vol. 129, pp. 30-44, 2018.

[7] W. Massey and J. Sunderland, "Heat and Mass Transfer in Semi-Porous Channels with Application to Freeze-Drying," *International Journal of Heat and Mass Transfer,* vol. 15, no. 3, pp. 193-502, 1972.

[8] G. Lusk, S. Goldblith and M. Karel, "Thermal Conductivity of Some Freeze-Dried Fish," *Food Technology,* vol. 18, no. 10, p. 1625, 1964.

[9] Y. Song and K. Sundmacher, "Approximation of Laminar Flow Field in Rectangular Channels with Suction/Injection Along One Wall," *Chemical Engineering Communications,* vol. 197, no. 4, pp. 551-570, 2009.

[10] Y. Cheng and G. Hwang, "Experimental Studies of Laminar Flow and Heat Transfer in a One-Porous-Wall Square Duct with Wall Injection," *International Journal of Heat and Mass Transfer,* vol. 38, no. 18, pp. 3475-3484, 1995.

[11] S. Zhang and J. Liu, "Distribution of Vapor Pressure in the Vacuum Freeze-Drying Equipment," *Mathematical Problems in Engineering,* 2012.

[12] M. Pettiti, A. Barresi and D. Marchisio, "CFD Modeling of Condensers for Freeze-Drying Processes," *Sadhana,* vol. 38, no. 6, pp. 1219-1239, 2013.

[13] A. Ganguly and A. Alexeenko, "Modeling and Measurements of Water-Vapor Flow and Icing at Low Pressures with Application to Pharmaceutical Freeze-Drying," *International Jouranl of Heat and Mass Transfer,* vol. 55, no. 21, pp. 5503-5513, 2012.

[14] A. Alexeenko, A. Ganguly and S. Nail, "Computational Analysis of Fluid Dynamics in Pharmaceutical Freeze-Drying," *Journal of Pharmaceutical Sciences,* vol. 98, no. 9, pp. 3483-3494, 2009.

[15] A. Alexeenko, A. Ganguly and S. Nail, "Use of Computational Fluid Dynamics for Improving Freeze-Dryers Design and Process Understanding. Part 2: Condenser Duct and Valve Modeling," *European Journal of Pharmaceutics and Biopharmaceutics,* vol. 129, pp. 45-57, 2018.

[16] A. Barresi, S. Velardi, R. Pisano, V. Rasetto, A. Vallan and M. Galan, "In-Line Control of the Lyophilization Process. A Gentle PAT Approach Using Software Sensors," *International Journal of Refrigeration,* vol. 32, no. 5, pp. 1003-1014, 2009.

[17] A. Barresi, R. Pisano, V. Rasetto, D. Fissore and D. Marchisio, "Model-Based Monitoring and Control of Industrial Freeze-Drying Processes: Effect of Batch Nonuniformity," *Drying Technology,* vol. 28, no. 5, pp. 577-590, 2010.

[18] A. Ganguly, N. Varma, P. Sane, R. Bogner, M. Pikal and A. Alexeenko, "Spatial Variation of Pressure in the Lyophilization Product Chamber Part 1: Computational Modeling," *AAPS PharmSciTech,* vol. 18, no. 3, pp. 577-585, 2017.

[19] T. Zhu, E. Moussa, M. Witting, D. Zhou, K. Sinha, M. Hirth, M. Gastens, S. Shang, N. Nere, S. Somashekar and A. Alexeenko, "Predictive Models of Lyophilization Process for Development, Scale-Up/Tech Transfer and Manufacturing," *European Journal of Pharmaceutics and Biopharmaceutics ,* vol. 128, pp. 363-378, 2018.

[20] V. Rasetto, D. Marchisio, D. Fissore and A. Barresi, "On the Use of a Dual-Scale Model to Improve Understanding of a Pharmaceutical Freeze-Drying Process," *Journal of Pharmaceutical Sciences,* vol. 99, no. 10, pp. 4337-4350, 2010.

[21] V. Rasetto, D. Marchisio, D. Fissore and A. Barresi, "Model-Based Monitoring of a Non-Uniform Batch in a Freeze-Drying Process," in *Proceedings of the 18th European Symposium on Computer-Aided Process Engineering-ESCAPE18*, 2008.

[22] P. Sane, N. Varma, A. Ganguly, M. Pikal, A. Alexeenko and R. Bogner, "Spatial Variation of Pressure in the Lyophilization Product Chamber Part 2: Experimental Measurements and Implications for Scale-Up and Batch Uniformity," *AAPS PharmSciTech,* vol. 18, no. 2, pp. 369-380, 2017.

[23] L. Wegiel, S. Ferris and S. Nail, "Experimental Aspects of Measuring the Vial Heat Transfer Coefficient in Pharmaceutical Freeze-Drying," *AAPS PharmSciTech,* vol. 19, no. 4, pp. 1810-1817, 2018.

[24] S. Nail, S. Tchessalov, E. Shalaev, A. Ganguly, E. Renzi, F. Dimarco, L. Wegiel, S. Ferris, W. Kessler, M. Pikal and G. Sacha, "Recommended Best Practices for Process Monitoring

Instrumentation in Pharmaceutical Freeze-Drying," *AAPS PharmSciTech,* vol. 18, no. 7, pp. 2379-2393, 2017.

[25] M. Pikal, M. Roy and S. Shah, "Mass and Heat Transfer in Vial Freeze-Drying of Pharmaceuticals: Role of the Vial," *Journal of Pharmaceutical Sciences,* vol. 73, no. 9, pp. 1224-1237, 1984.

[26] E. Liechty, A. Strongrich, E. Moussa, E. Topp and A. Alexeenko, "In-Situ Molecular Vapor Composition Measurements During Lyophilization," *Pharmaceutical Research,* vol. 35, no. 6, p. 115, 2018.

[27] A. Hottot, J. Andrieu, V. Hoang, E. Shalaev, L. Gatlin and S. Ricketts, "Experimental Study and Modeling of Freeze-Drying in Syringe Configuration Part II: Mass and Heat Transfer Parameters and Sublimation End-Points," *Drying Technology,* vol. 27, no. 1, pp. 49-58, 2009.

[28] W. Wagner and A. Pruß, "The IAPWS Formulation 1995 for the Thermodynamic Properties of Ordinary Water Substance for General and Scientific Use," *Journal of Physical and Chemical Reference Data,* vol. 31, no. 2, pp. 387-535, 2002.

[29] G. Shivkumar, P. Kazarin, A. Strongrich and A. Alexeenko, "LyoPRONTO: An Open-Source Lyophilization Process Optimization Tool," *AAPS PharmSciTech,* vol. 20, no. 8, p. 328, 2019.

[30] M. Pikal, "Use of Laboratory Data in Freeze Drying Process Design: Heat and Mass Transfer Coefficients and the Computer Simulation of Freeze Drying."," *PDA Journal of Pharmaceutical Science and Technology,* vol. 39, no. 3, pp. 115-139, 1985.

[31] S. Velardi and A. Barresi, "Development of Simplified Models for the Freeze-Drying Process and Investigation of the Optimal Operating Conditions."," *Chemical Engineering and Research and Design,* vol. 86, no. 1, pp. 9-22, 2008.

[32] W. Mascarenhas, H. Akay and M. Pikal, "A Computational Model for Finite Element Analysis of the Freeze-Drying Process," *Computer Methods in Applied Mechanics and Engineering,* vol. 148, no. 1, pp. 105-124, 1997.

[33] W. Kuu, K. O'Bryan, L. Hardwick and T. Paul, "Product Mass Transfer Resistance Directly Determined During Freeze-Drying Cycle Runs Using Tunable Diode Laser Absorption Spectroscopy (TDLAS) and Pore Diffusion Model," *Pharmaceutical Development and Technology,* vol. 16, no. 4, pp. 343-357, 2011.

[34] S. Ehlers, R. Schroeder and W. Freiss, "Trouble With the Neighbor During Freeze-Drying: Rivalry About Energy," *Journal of Pharmaceutical Sciences,* vol. 110, no. 3, pp. 1219-1226, 2021.

[35] A. Barresi, "Use of CFD for the Design and Optimization of Freeze-Dryers," in *Freeze Drying of Pharmaceutical Products*, CRC Press, 2019.

[36] A. Barresi, R. Pisano, D. Fissore, Rasetto, S. Velardi, A. Vallan and M. Parvis, "Monitoring of the primary drying of a lyophilization process in vials," *Chemical Engineering and Processing: Process Intensification,* vol. 48, no. 1, pp. 408-423, 2009.

[37] R. Pisano, D. Fissore and A. Barresi, "Freeze-Drying Cycle Optimization Using Model Predictive Control Techiques," *Industrial and Engineering Chemistry Research,* vol. 50, no. 12, pp. 7363-7379, 2011.

1

2

Table 1: Summary of conducted experiments. All changes in shelf temperature are conducted at a rate of 1°C/min. Cycle H was performed twice to investigate the effects of lyophilizer configuration, once with sidewall flow barriers and once without.

Cycle	Formulation	Fill Volume	Freezing	Primary Drying		Secondary Drying	
			Shelf Temperature	Chamber Pressure	Shelf Temperature	Chamber Pressure	Shelf Temperature
A	Water	5 mL	1 hr @ -40°C	9.3 Pa	-20 °C	N/A	N/A
B	5% w/v Sucrose	5 mL	1 hr @ -40°C	9.3 Pa	-20 °C	9.3 Pa	40 °C
C	5% w/v Sucrose	5 mL	1 hr @ -40°C	9.3 Pa	-10 °C	9.3 Pa	40 °C
D	5% w/v Sucrose	5 mL	1 hr @ -40°C	9.3 Pa	10 °C	9.3 Pa	40 °C
E	5% w/v Sucrose	5 mL	1 hr @ -40°C	13.3 Pa	10 °C	13.3 Pa	40 °C
F	5% w/v Sucrose	5 mL	1 hr @ -40°C	20.0 Pa	10 °C	20.0 Pa	40 °C
G	5% w/v Mannitol	5 mL	0 hr @ -40°C 3 hr @ -15°C 1 hr @ -40°C	9.3 Pa	-20 °C	9.3 Pa	40 °C
H	5% w/v Mannitol	5 mL	0 hr @ -40°C 3 hr @ -15°C 1 hr @ -40°C	13.3 Pa	10 °C	13.3 Pa	40 °C
I	5% w/v Mannitol	5 mL	0 hr @ -40°C 3 hr @ -15°C 1 hr @ -40°C	13.3 Pa	-10 °C	13.3 Pa	40 °C

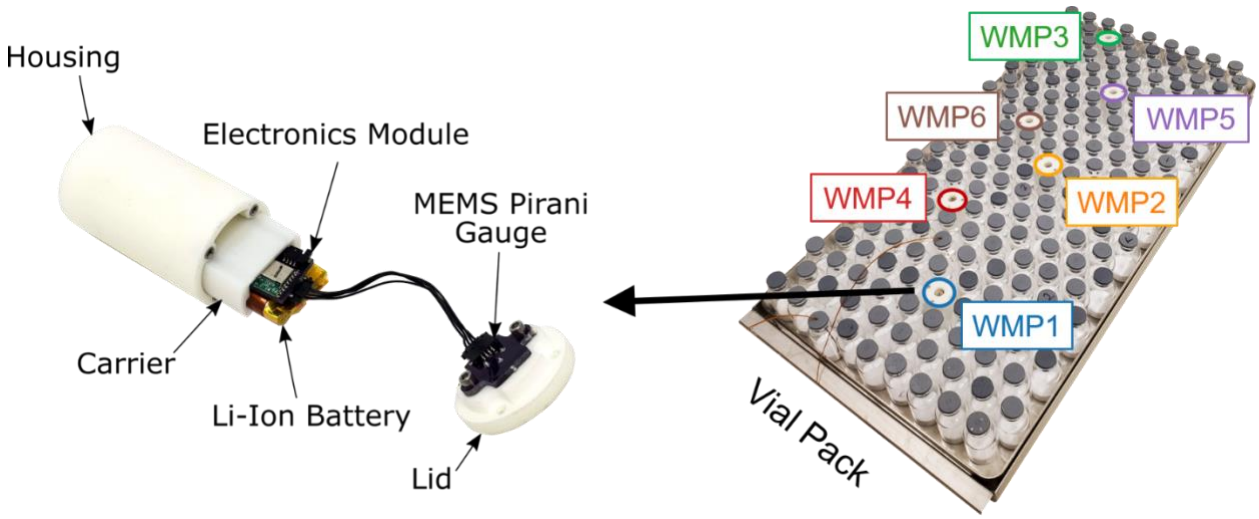

Figure 1: Schematic of Wireless MicroPirani (WMP) sensor (left) and device locations within the vial pack during experiments (right). The staggered linear arrangement shown was maintained during all experiments to capture axial and transverse gradients.

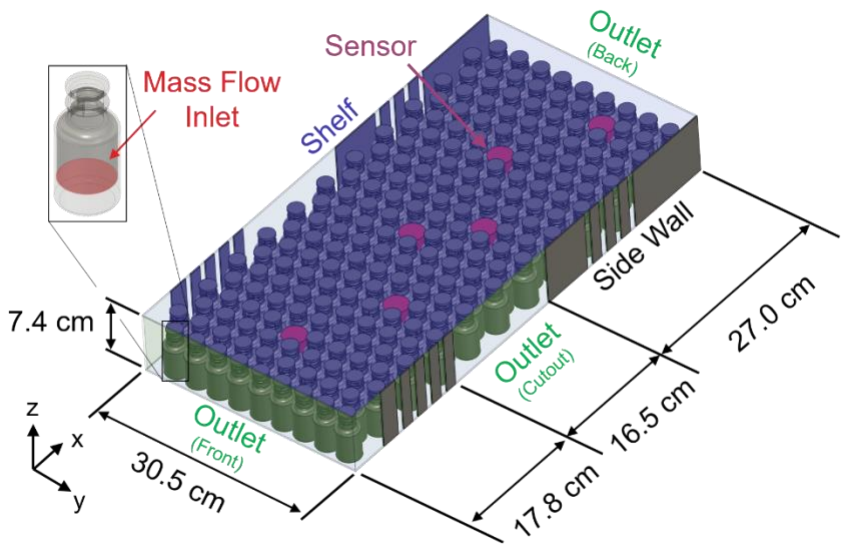

Figure 2: Schematic of CFD domain modeled after REVO® lyophilizer. Sensor locations are matched to physical placement within vial pack (see Figure 1) to facilitate direct comparison. All vials are assumed to have identical sublimation rates and inlet temperatures.

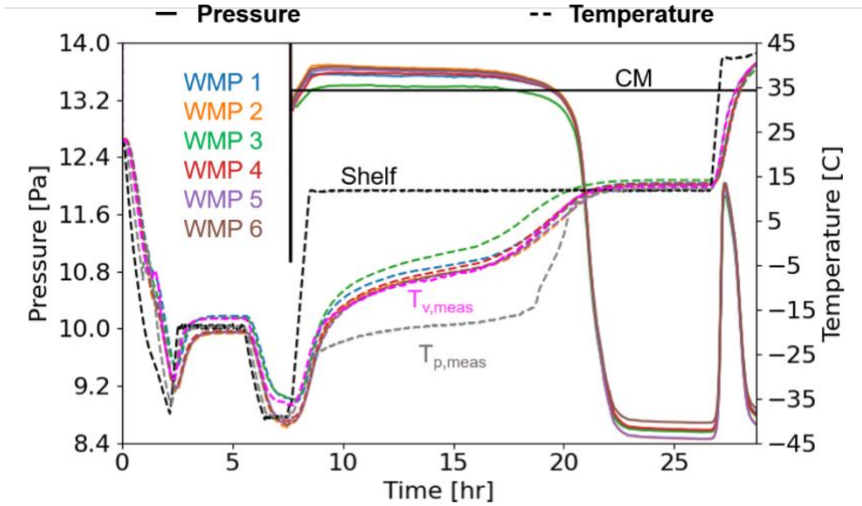

Figure 3: Summary of process and WMP data from Cycle H. Pressure and temperature data are indicated by solid and dashed lines, respectively. WMP measurements are coded by color and can be correlated to the positions indicated in Figure 1.

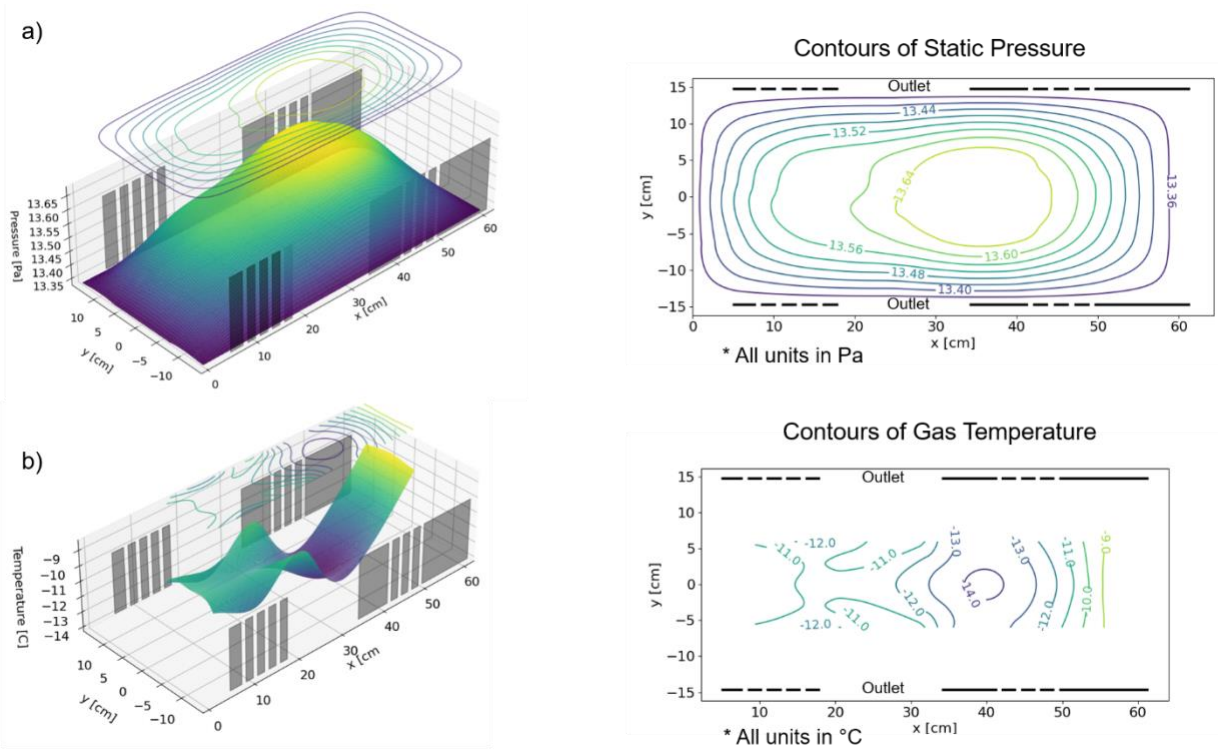

Figure 4: Experimentally derived pressure (a) and temperature (b) maps during lyophilization of a 5% w/v mannitol formulation at a chamber pressure of 13.3 Pa and shelf temprature of 10°C (Cycle H in Table 1). The surface data is represented as contours on the right side of the figure. The locations of the sidewall cutouts are included to demonstrate their influence on the flowfield. The base chamber pressure of 13.3 Pa was assumed along the periphery of the pressure contour. Temperature information at these locations was not measured and therefore cannot be filled.

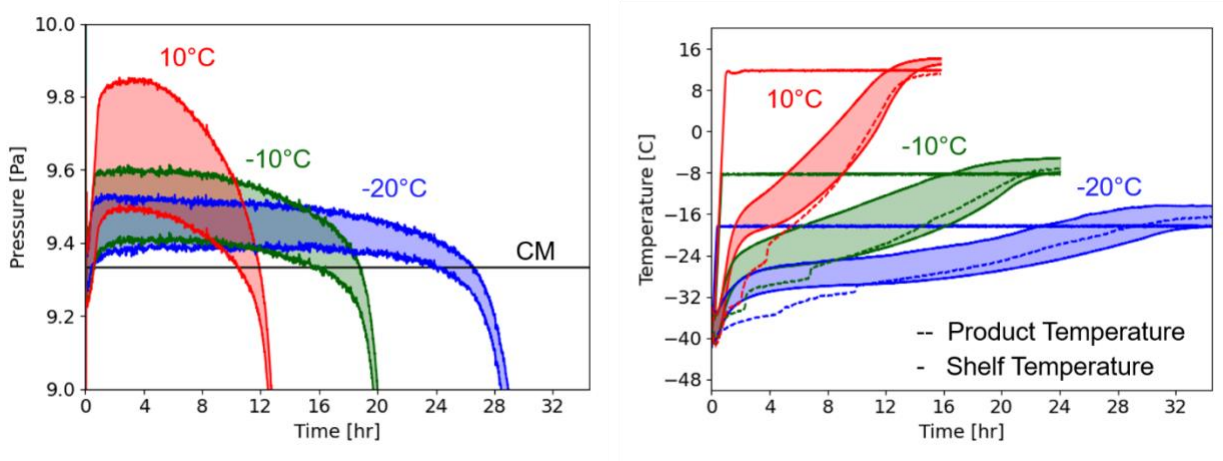

Figure 5: Effect of shelf temperature on local pressure (left) and temperature (right) during primary drying of 5% w/v sucrose (Cycles B,C,D in Table 1). The upper and lower bounds on the shaded envelopes indicate the process variable measurements at the center (WMP2) and aft (WMP3) edge of the shelf, respectively. Increasing shelf temperature leads to an increase in sublimation rate which leads to a greater pressure difference from center to edge.

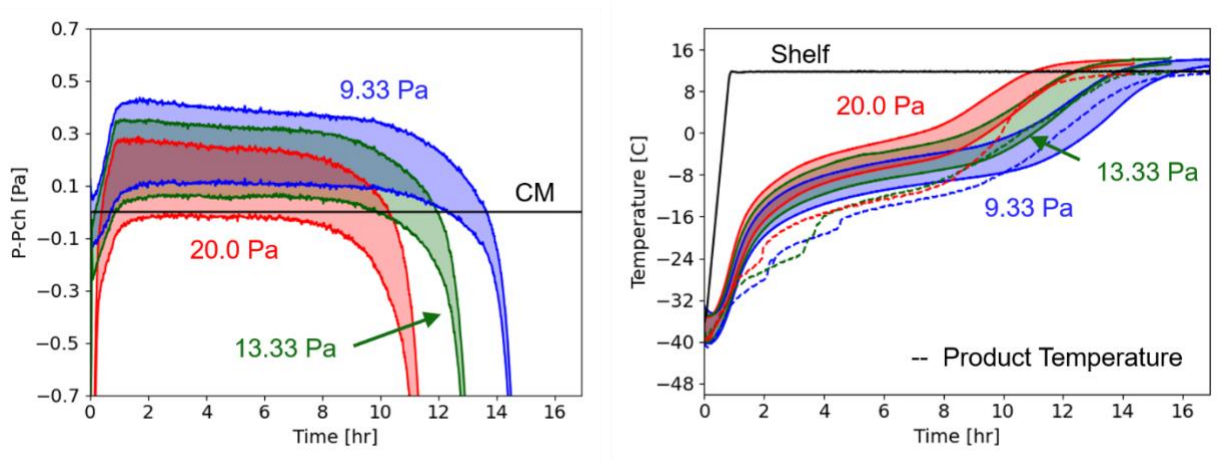

Figure 6: Effect of chamber base pressure on local pressure (left) and temperature (right) during primary drying of 5% w/v sucrose (Cycles D, E, and F in Table 1). The upper and lower bounds on the shaded envelopes indicate the process variable measurements at the center (WMP2) and aft (WMP3) edge of the shelf, respectively. The pressure difference is represented as the gauge pressure relative to the chamber pressure to facilitate direct comparison. Increasing chamber pressure leads to a decrease in the pressure drop from the center of the shelf to the edge due to increase in Reynolds number. The chamber pressure directly modulates the heat transfer at low pressures characteristic of lyophilization, resulting in a higher gas temperature over the course of primary drying.

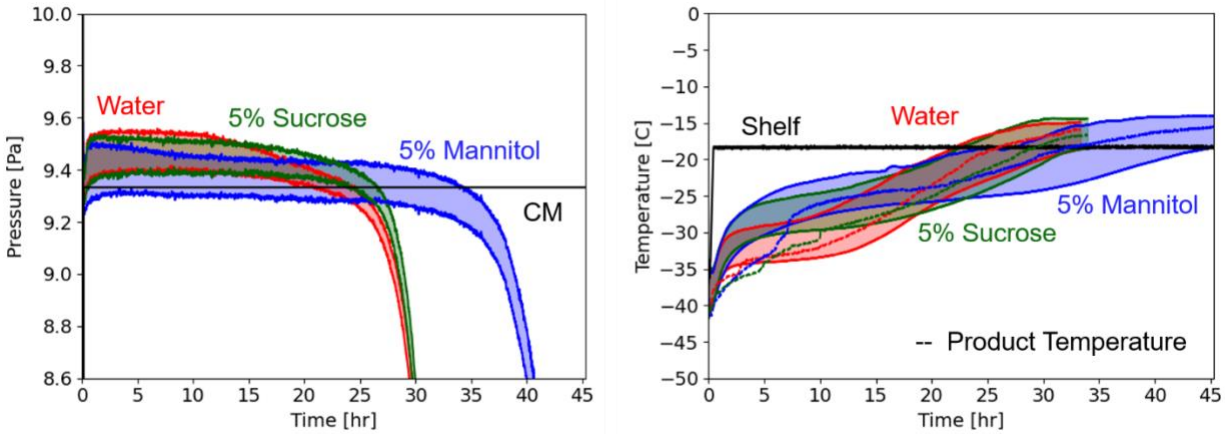

Figure 7: Effect of excipient on local pressure (left) and temperature (right) during primary drying (Cycles A, B, and G). The upper and lower bounds on the shaded envelopes indicate the process variable measurements at the center (WMP2) and aft (WMP3) edge of the shelf, respectively. Samples containing only water sublime most quickly due to the absence of a dry layer. Mannitol experiences the lowest drying rate due to its resistance to microcollapse. Local backstreaming and mixing of the ballast and water vapor most likely contributes to the indicated edge pressure being lower than the chamber pressure for the mannitol formulation. In terms of gas temperature, water produces the lowest overall magnitudes due to its high sublimation rate which offsets the conduction heat transfer from the shelves.

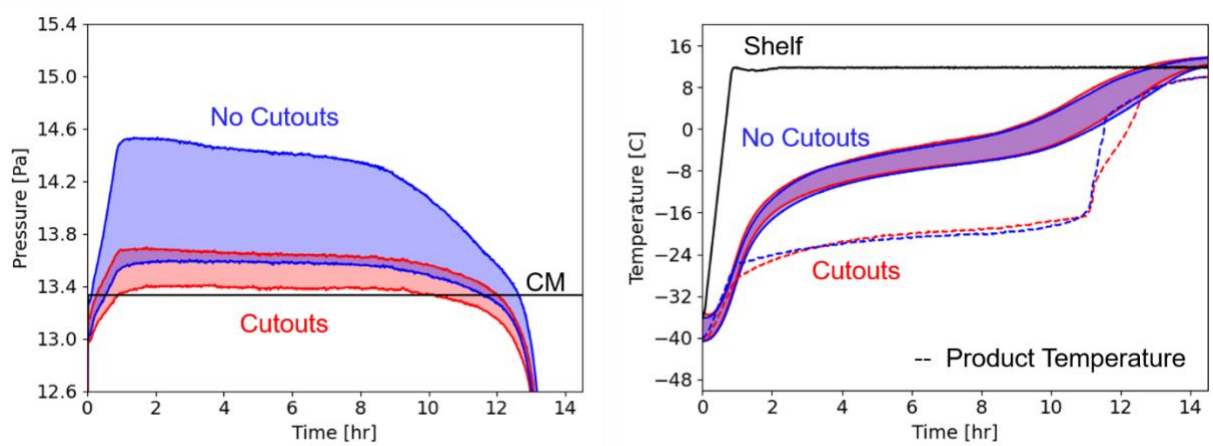

Figure 8: Effect of lyophilizer configuration on local gas pressure (left) and temperature (right) during primary drying of 5% w/v mannitol (Cycle H in Table 1). The upper and lower bounds on the shaded envelopes indicate the process variable measurements at the center (WMP2) and aft (WMP3) edge of the shelf, respectively. The absence of sidewall cutouts leads to a significant increase in pressure gradient along the centerline. The vial heat transfer coefficient is relatively insensitive to pressure variations of this magnitude at the indicated base pressure and therefore the lyophilizer configuration has a relatively minimal impact on drying rate.

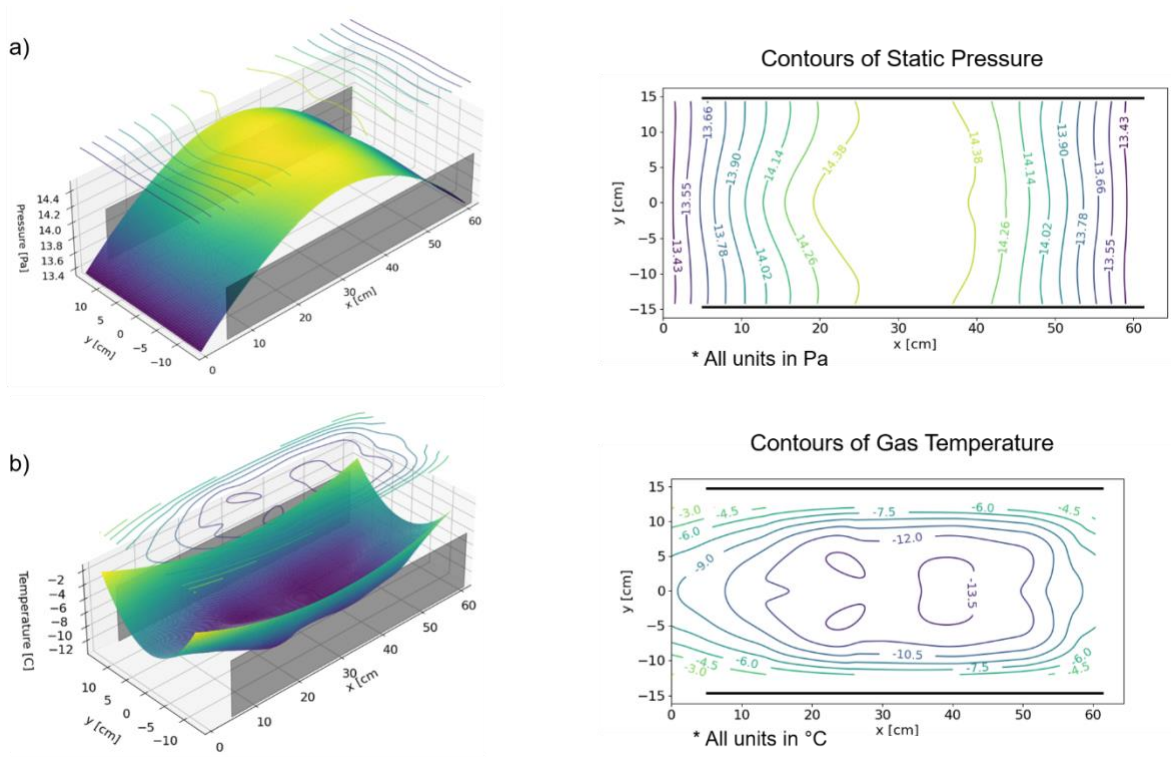

Figure 9: Experimentally derived pressure (a) and temperature (b) maps during lyophilization of a 5% w/v mannitol formulation at a chamber pressure of 13.3 Pa and shelf temprature of 10°C (Cycle H in Table 1) using flow barriers along the shelf sidewalls. The surface data is represented as contours on the right side of the figure. The barriers constrain the flow to leave the domain at the fore and aft exits only. This attenuates transverse pressure gradients (y-direction) and makes the system approximately 2-dimensional.

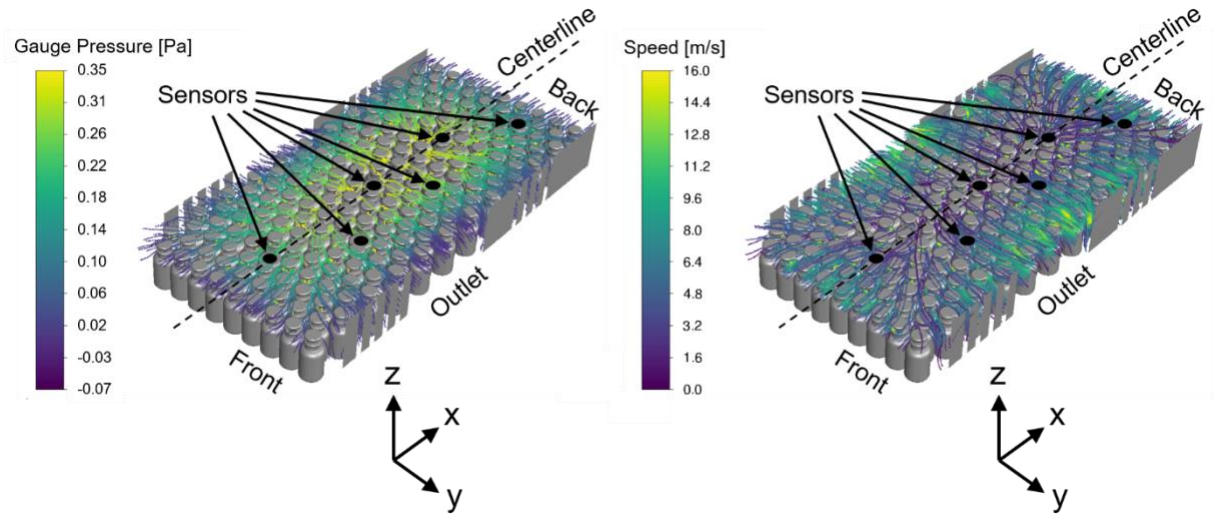

Figure 10: Flow pathlines colored by gauge pressure (left) and vapor speed (right) determined from CFD simulations of 5% w/v mannitol dried at a chamber pressure of 13.3 Pa and shelf temperature of 10°C (Cycle H in Table 1). Pressure contours are in qualitative agreement with experimental measurements in Figure 4. Water vapor exits the vials and proceeds along the directions of highest pressure gradient magnitude. Gradients near the center are strong towards the sidewall cutouts in the y-

direction and cause a large quantity of fluid to egress at these locations with high velocity. This redistribution of mass flow leads to the lower pressure drop from center to edge seen in Figure 8.

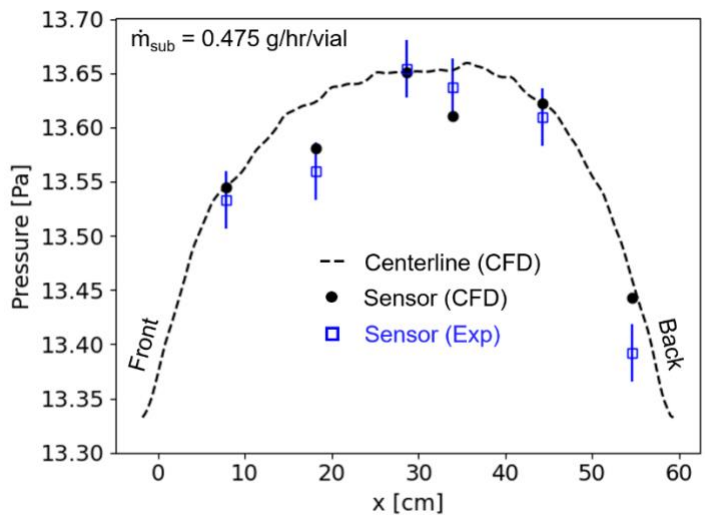

Figure 11: Comparison of experimental and calculated pressure within the vial pack for a 5% w/v mannitol formulation (Cycle H in Table 1) at a process time of 11 hours as determined from the sublimation rate estimation procedure. Sensor locations from front to back are indicated in Figures 1, 2, and 10.

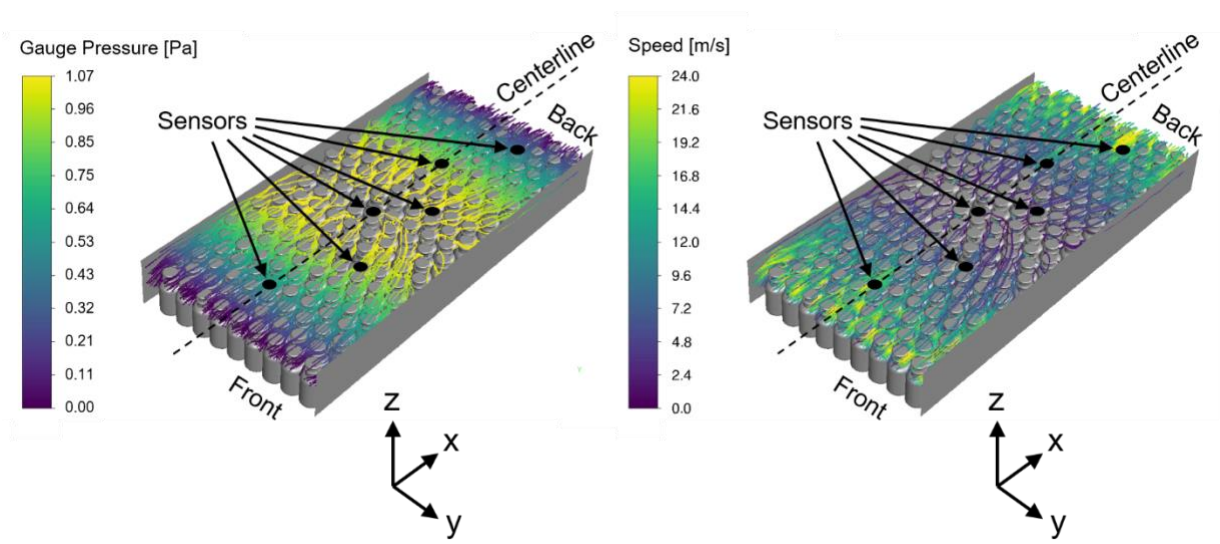

Figure 12: Flow pathlines colored by gauge pressure (left) and vapor speed (right) determined from CFD simulations of 5% w/v mannitol dried at a chamber pressure of 13.3 Pa and shelf temperature of 10°C (Cycle H in Table 1) with flow barriers. Pressure contours are in qualitative agreement with experimental measurements in Figure 9 and exhibit variation along the shelf axis only. The reduced overall cross sectional exit area increases the flow rate demand and leads a larger exit velocity magnitude relative to the case with cutouts by around 50%.

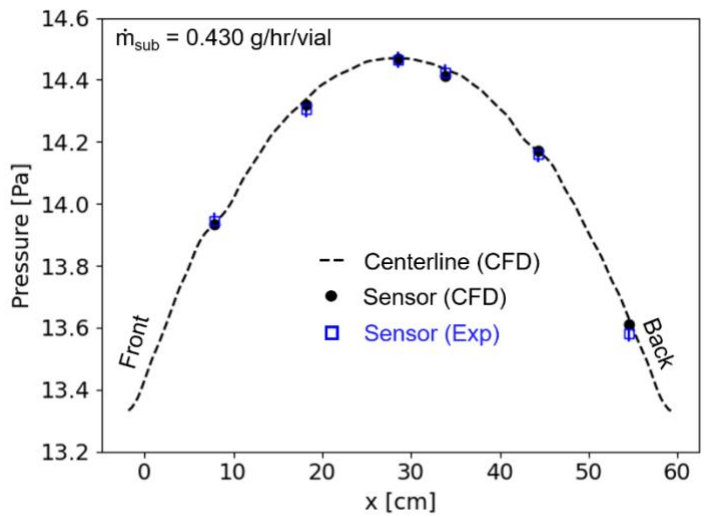

Figure 13: Comparison of experimental and calculated pressure within the vial pack for a 5% w/v mannitol formulation (Cycle H in Table 1) using flow barriers at a process time of 11 hours as determined from the sublimation rate estimation procedure. Sensor locations from front to back are indicated in Figures 1 and 2. All sensors demonstrate good agreement with the CFD solution and fall within the calibration uncertainty bounds.

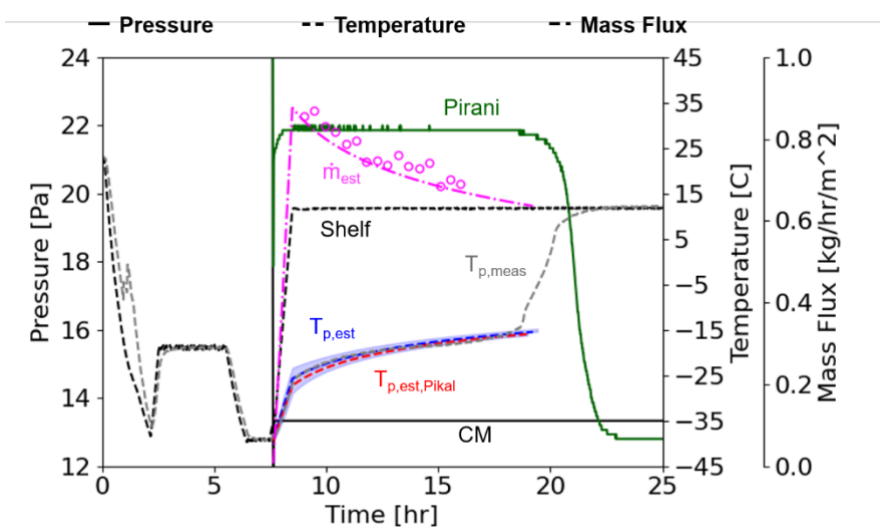

Figure 14: Estimated product temperature and mass flux following heat and mass transfer characterization for cycle H without flow barriers. Temperature estimates based on the mass transfer resistance correlation developed by Pikal et al.[25] for 5% w/v mannitol are also shown. Open circles represent the sublimation rate obtained by matching experimentally measured pressure to the CFD results.